SCIENTIFIC REPORTS

OPEN

Pore cross-talk in colloidal filtration

Olivier Liot[1,2,6], Akash Singh[1], Patrice Bacchin[3], Paul Duru[4], Jeffrey F. Morris[5] & Pierre Joseph[1]

Received: 23 April 2018
Accepted: 27 July 2018
Published online: 20 August 2018

Blockage of pores by particles is found in many processes, including filtration and oil extraction. We present filtration experiments through a linear array of ten channels with one dimension which is sub-micron, through which a dilute dispersion of Brownian polystyrene spheres flows under the action of a fixed pressure drop. The growth rate of a clog formed by particles at a pore entrance systematically increases with the number of already saturated (entirely clogged) pores, indicating that there is an interaction or "cross-talk" between the pores. This observation is interpreted based on a phenomenological model, stating that a diffusive redistribution of particles occurs along the membrane, from clogged to free pores. This one-dimensional model could be extended to two-dimensional membranes.

A colloidal suspension flowing through a pore network often results in fouling or clogging. In industrial (oil recovery[1], inkjet printing[2], filtration), biological (artery diseases[3], detection of cells[4]) and natural (water infiltration in soils[5], precipitation inside rocks[6]) processes, the phenomenon of particle accumulation is involved. Recent improvements in visualization of suspended particles in model pores have led to new insight into the physical parameters at play in particle capture and clogging in pores[7]. There are several different clogging mechanisms. Size exclusion or sieving occurs when particles block a pore smaller than their diameter[8]. If the pore size is larger than the particle, clogging can occur by two routes, either through particles forming an arch at the entrance of the pore[9] or progressively adhering to walls and previously deposited particles, leading to blockage of the pore[10,11]. During the last decade, following an early study[10] which described clogging of pores by smaller particles, a number of studies have focused on determining the pore-scale mechanisms involved in this form of pore blockage (e.g.[12–17]). Other studies have proposed explanations of clogging using transition-state theory[18] or by relating it to jamming phenomena[19].

Prior to the advent of pore-scale investigations, which have been greatly facilitated by microfluidic technology, numerous studies were made at a more macroscopic membrane scale, where the usual focus was on the "filtration cake"[20–24]. Since a typical filtration membrane consists of a large number of closely-spaced pores, clog formation at one pore could affect its neighbours, and hence the macroscopic behavior of the membrane. Considered in this way, there is a notable lack of information related to clog formation at the pore scale, with connection to the membrane scale by consideration of interactions between pores. In this work, we address this gap of knowledge at an intermediate scale, by considering in detail the time evolution of the clog formation process at pore scale, in a short one-dimensional (1-D) array of pores. We describe the interaction between pores as "cross-talk". While one recent paper[18] shows that a filtration cake can overhang neighbouring pores and influence the clog formation, there is, to our knowledge, no direct analysis of the pore cross-talk phenomenon. Yet it could have a dramatic impact on the understanding of filtration process of suspensions at macroscale, such as possible preferential locations of cake formation.

In this work, we present observations of cross-talk when a Brownian suspension flows through a 1-D microfiltration device. The flow is driven by a fixed pressure difference, not a fixed flow rate, and this is a key point of our study. We measure a clogging growth rate as a function of the number of already clogged pores and we propose a model based on a local increase of colloid concentration close to clogged pores to explain the observations.

Experimental Methods

Ten nanoslits of width $w = 5\,\mu$m, length $L = 50\,\mu$m, depth $h = 830$ nm, and center-to-center spacing $\delta = 20\,\mu$m are etched in silicon. These nanoslits connect much larger inlet and outlet rectangular microchannels acting as reservoirs (depth 23 μm, width 100 μm and millimetric in the third direction). The device is covered with a 170 μm -thick borosilicate glass plate. The design is presented in Fig. 1 (left) which shows that the nanoslits connect

[1]LAAS-CNRS, Université de Toulouse, CNRS, Toulouse, France. [2]Fédération FERMaT, INP, Toulouse, France. [3]Laboratoire de Génie Chimique, Université de Toulouse, CNRS, Toulouse, France. [4]Institut de Mécanique des Fluides de Toulouse, Université de Toulouse, CNRS, Toulouse, France. [5]Levich Institute and Chemical Engineering, CUNY City College of New York, New York, USA. [6]Present address: Institut Lumière Matière, CNRS, Villeurbanne, France. Correspondence and requests for materials should be addressed to O.L. (email: olivier.liot@ens-lyon.fr)

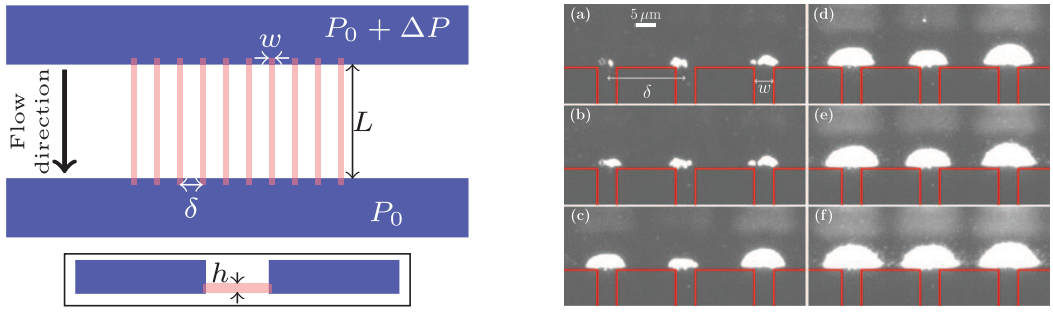

Figure 1. Sketch of the model pores and micrograph of some clogs. Left: top view of the chip design with zoom on nanoslits. Microchannels are represented in blue, nanoslits in red. Inset: side view of the nanoslits (not to scale). Right: image of the development of three adjacent clogs at the entrance of pores. Red lines delimit the nanoslits. For (**a**) to (**f**) the corresponding times are t = 1333, 2000, 2666, 3000, 3333, 4000 s.

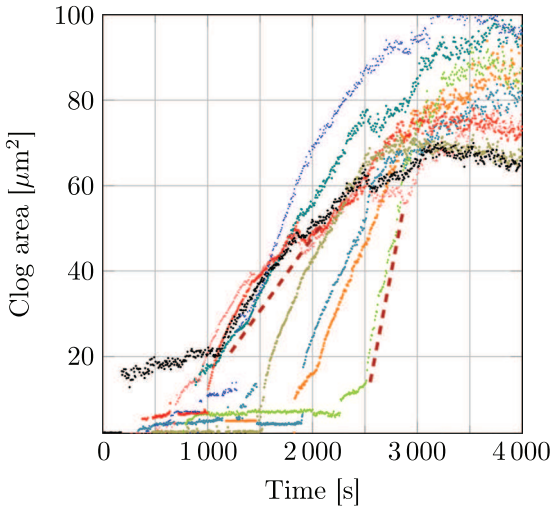

Figure 2. Time evolution of clogs area during a single acquisition. Drawn lines highlight the zone where clog growth rate is estimated.

corners of the cross-section of the microchannels. The channels are filled with a suspension of $d_p = 250$ nm diameter polystyrene particles (density 1.05 g.cm^{-3}). The particles are carboxylate-modified and dispersed in a solution of monovalent phosphate buffered saline (PBS) diluted to an ionic strength $I = 3$ mM. The zeta potential ζ_p is measured by laser Doppler electrophoresis, $\zeta_p = -69$ mV (pH = 7.5). The volume fraction of the suspension is $\phi_0 = 3.8 \times 10^{-5}$. A pressure difference of $\Delta P = 20 \pm 0.02$ mbar is applied across the length of the nanoslits using a controller device. Experiments are made in dead-end and slow crossflow filtration (with velocity 0 to 9 μm/s at 2 μm from the entrance of the pores).

The clogging dynamics are observed using wide field fluorescence microscopy with a 40× magnification and 1.4 numerical aperture objective. Since the characteristic time for clogging is found to be about one hour we acquire images of the clog growth process at a frequency of 90 frames per minute. Figure 1 (right) shows an example of the development of three adjacent clogs. The contour of the aggregated particle mass is detected using custom *Python* scripts. From this contour analysis, we are able to determine the projected area of each clog in the field of view.

An experimental difficulty is caused by the very low flow rate involved: the total flow rate through the ten pores before clogging is about 5 nL.min^{-1}, well below the sensitivity limit of commercial flow rate sensors. Tracking of particles inside nanoslits while acquiring clog development is also technically difficult. Timescales are indeed very different (20 ms is the typical residence time of particles in the nanoslits versus a typical clog growth of one hour). Moreover the brightness of one single particle compared to a clog of hundreds of colloids makes hard to capture simultaneously individual colloids and clogs. Perfect watertight fitting of the chip to the pressure controller must be ensured. Also, the chips can often not be retrieved after an experiment: a clogged chip is often discarded.

Results

Experimental observations. Figure 2 shows an example of the time evolution of the area of aggregated particles at each of the pore entrances in a single microfluidic chip. The curves all display the same characteristic shape. After an initial time period where the curves are quite uneven, each shows a rapid quasi-linear growth up to a saturation level. In the present experiment, pore clogging is mainly initiated by the capture of particle

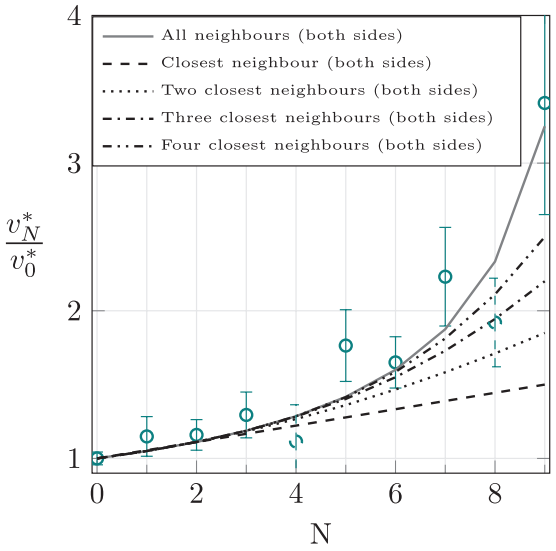

Figure 3. v_N^*/v_0^* ratio versus N. The error bars are related to statistical uncertainty (standard deviation over root square of the number of events); dashed points are low statistic points (less than three events). The different lines show the predictions of Eq. 3, with different ways of computing $\langle k \rangle_N$, see legend for details.

aggregates. This is not surprising as the ratio nanoslit height/particle diameter is only 3.3. Also, the presence of small aggregates in the suspension cannot be ruled out even if care is taken to prevent the aggregate presence (by sonicating the suspension prior to its use). The larger of these aggregates can sometimes be identified on the images, at the nanoslit entrance, once they have been captured. Aggregates partially obstruct the pore and then initiate the slow clog growth sometimes visible at the beginning of the clogging, see e.g. the black and blue data points in Fig. 2. When the pore is fully blocked, all the particles are sieved from the flow and most are captured on the aggregate (some may move laterally) so that the clog begins its fast-growth phase. The saturation of the clog is apparently due to a balance between drag (note that the flow rate through a pore decreases when the clog grows, leading to a decrease of the drag force exerted on the particles) and the combination of double layer repulsion and Brownian diffusion, resulting in a zero particle flux surface, similar to the situation described by Bacchin *et al.*[12]. We note that this balance between transport mechanisms is the one classically put forward to explain the existence of a stationary concentration polarization layer in filtration of colloidal suspensions[25,26]. An analogous equilibrium (fluid flow-induced drag forces vs diffusiophoretic flow-induced ones) has been observed recently[27]. Note that in the case of an experiment performed with a fixed flow rate (in contrast with the present fixed pressure drop configuration), no saturation of the clog size would be observed: particles would continue to accumulate indefinitely on the clog[18].

In the present paper, neither a precise description of the clogging dynamics at the pore scale nor a quantitative description of the saturation mechanisms are the objectives of the study (note studies of clogging at pore scale in conditions similar to that of the experiments have already been performed[11,12,14]). We rather focus on the following observation: when a clog begins its rapid growth after other pores have reached saturation, the growth rate is larger: e.g., compare the green and black curves in Fig. 2. The goal of the paper is to describe quantitatively and to model this observation.

We quantitatively define clog growth rate (with dimensions of area/time) as the average of the derivative of the measured area with time in the zone starting from the beginning of the fast growth part where its evolution is linear, see Fig. 2 (more details on the data processing are given as Supplementary materials 1). We made eight acquisitions, totaling 80 growth rate measurements. We define the mean growth rate when N pores are saturated (i.e. clog size has reached saturation) as v_N^*. We have $N \in [0, N_{tot} - 1]$ where N_{tot} is the total number of pores. Note that during an experiment, two or more pores may start to clog nearly simultaneously. Consequently, for a given experiment, all values of N are not necessarily observed. As an example, if the two first pore-clogging events are simultaneous, the data for the third one will count as an $N = 2$ event and such an experiment lacks a $N = 1$ event. Figure 3 displays the ratio v_N^*/v_0^* as a function of N. Despite some large error bars, a clear increase of v_N^*/v_0^* is observed when the number of saturated pores increases, from $v_N^*/v_0^* = 1$ for $N = 0$ to $v_N^*/v_0^* \approx 3$ for $N = 9$. As already mentioned, explaining this increase of v_N^*/v_0^* with N is the main goal of this paper and we now propose a phenomenological model.

Phenomenological model. Clog growth rate is proportional to the flow rate through a free pore Q_f and the local concentration of particles[10]. Two mechanisms can explain the growth rate rise: particle concentration increase and/or flow rate increase. In the present fixed pressure-drop configuration, we assume that the flow rate through a free pore, Q_f, remains constant as long as clogging did not begin and that a saturated clog acts as a filter, with fluid permeating through it at a flow rate $Q_s < Q_f$.

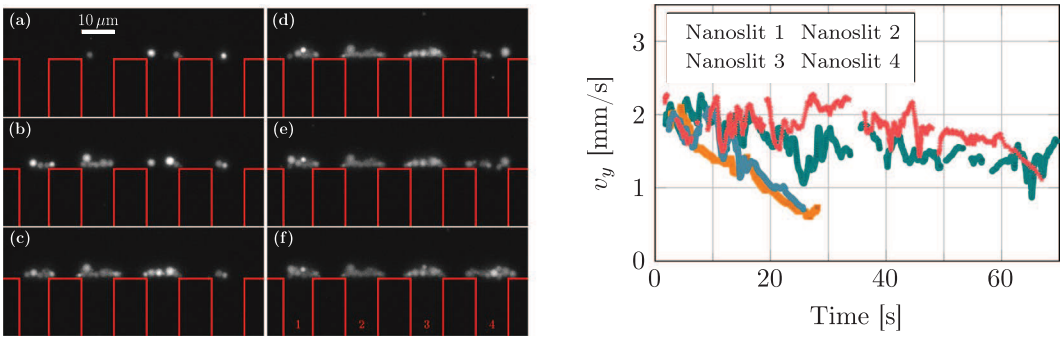

Figure 4. Left: image of the development of four adjacent polymersome clogs at the entrance of pores. Red lines delimit the nanoslits. For (**a**) to (**f**) the corresponding times are t = 0, 14, 28, 42, 56, 70 s. Right: Sliding average of instantaneous longitudinal velocities of multiple polymersomes flowing through each nanoslit versus time. Nanoslits numbers correspond to numbers written on the left figure (**f**).

In the present experiment, an estimate of the flow rate within a free pore cannot be obtained easily (see Experimental methods). However, we now present some data from another experiment supporting the above assumptions. These experiments are performed in micro-system similar to those used in the present study (only two dimensions of the nanoslits change: 1650 nm in height and 10 μm in width), where a dilute suspension of self-assembled objects made of polymers (polymersomes) is flowed through the nanoslits (for more details see Liot *et al.*[28]). These polymersomes can be tracked and their instantaneous longitudinal velocities recorded. Because of the polydispersity of such objects, some of them are larger than the nanoslits height and can clog them quickly, as presented in Fig. 4 (left). Figure 4 (right) shows a sliding average of the instantaneous longitudinal velocities v_y of tracked polymersomes flowing through each nanoslit. Two different behaviors are observed: a strong decrease of the velocity (and thus of the flow rate) for nanoslits 2 and 3 and a less pronounced decrease for nanoslit 2 and 4, for which clogging is not as rapid. Performed with a similar flow control than the present experiments, these data show that an increase of the flow rate can be ruled out in the present experiments with colloids. Furthermore the nanoslit 4 reveals constant polymersomes longitudinal velocity up to $t = 35$ s, when clogging becomes dramatic. Whereas the neighbouring pore (nanoslit 3) is blocked, no decrease of the flow rate in nanoslit 4 can be observed. We conclude that Q_f remains constant in a free pore during the filtration process. Since an increase of flow rate is excluded, the main idea of the present model is that the particles driven by the permeation flow close to a clogged pore will be "redistributed" along the membrane surface to flow through open pores, leading to a particle concentration increase close to a free pore.

A possible mechanism to explain this redistribution is Brownian diffusion. The typical time scale t^* between two successive pore clogging events is about 100 s (see Fig. 2). The diffusion coefficient of the particles at ambient temperature is[29] $D = 1.7 \times 10^{-12}$ m^2.s^{-1}. Their typical displacement during this time interval in one direction is $\delta x = \sqrt{2Dt^*} = 18$ μm. This typical length scale rises to about 60 μm when considering a typical experiment duration, $\mathcal{O}$(1000 s). Therefore, particle diffusive redistribution is expected to be a relevant mechanism in the present experiments. Note these estimates are obtained by using the diffusion coefficient for an isolated particle. Close to a clog ($\sim$100 nm), one may certainly expect diffusive transport to be affected by the particle-particle interactions, but this is not the case regarding the diffusive transport along the membrane, from a saturated to a free pore, where the particle concentration is expected to be close to the bulk concentration ϕ_0. Also, convective effects are expected to play a role. For instance, the flow rate decrease in pores with a saturated clog will lead to thinner stream tubes "feeding" these pores, and to larger ones for free pores. And it is enough for the particles to diffuse until they are "caught by" a stream tube flowing into a free pore. Secondary flows induced by clog spatial extension over the membrane could also have a similar effect, providing a convective component to the redistribution mechanism. However, as made clear below, it is crucial to understand that the model described later is not affected by the details of the redistribution mechanism.

This redistribution of particles is limited: all the particles redistributed from a saturated pore will be "sucked down" by the first free pores (on both sides of the saturated pore). In fact, in the case of a diffusive redistribution mechanism, advection of a particle through an open pore is much stronger than the diffusive transport away from it. This can be appreciated by building a Péclet number using the particle diameter and a typical flow velocity U: $Pe = 3\pi\eta d_p^2 U/k_B T$. A typical velocity within the nanoslit can be taken as $U_f = Q_f/(hw)$, where Q_f is computed from velocity field through a channel with rectangular cross-section with $\Delta P = 20$ mbar[30]. Away from the nanoslit, a typical velocity in the flow stream that will end up flowing through the nanoslit can be estimated as $U_f \times (h \times w)/(\delta \times 23\,\mu\text{m})$, which is $\approx U_f/50$. The Péclet is finally in the range 6–300, taking the typical velocity U in the range $U_f/50 - U_f$, showing that a particle will not be able to diffuse across a free pore, but will be captured by the flow into it. To strengthen this point, we compute the probability, when a pore saturates, that the next one to clog is at a distance Δx and observe a deviation from a stochastic process only for one inter-pore distance (see Fig. 2 in Supplementary materials).

We now propose a stationary phenomenological model to estimate the influence of the redistributed particles on clog growth rate. Assume that a free pore has k successive neighbouring saturated pores, including left and right directions. Figure 5 sketches the physical configuration for a $k = 2$ case, with the two clogs saturated on the

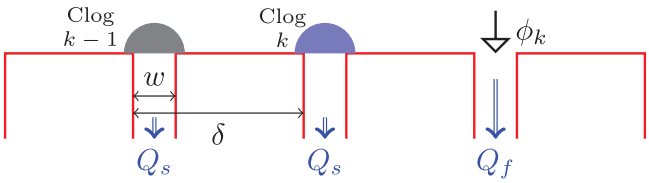

Figure 5. Sketch of a situation with two saturated pores neighbouring a free pore (therefore, $k=2$).

left side of the considered free pore. Each saturated pore acts as a source of particles diffusing in both directions away from the clog, toward the closest free pores. Only the growth rate of these first pores will be influenced by the saturated ones. The effective concentration of the suspension flowing through a free pore will be simply

$$\phi_k = \phi_0\left(1 + k\frac{Q_s}{2Q_f}\right), \tag{1}$$

each neighbouring clogged pore contributing equally to ϕ_k in the present model. However, the variable k is not easily available: it is specific to each free pore, depending on its environment which changes with time, and it depends on the configuration of free and saturated pores. Thereby, this problem has a statistical facet. When N pores out of N_{tot} are saturated, the effective concentration of the suspension flowing in a given opened pore, averaged over all opened-clogged pores configurations is defined as:

$$\langle\phi_k\rangle_N = \phi_0\left(1 + \langle k\rangle_N\frac{Q_s}{2Q_f}\right), \tag{2}$$

where $\langle k\rangle_N$ is the average number of neighbouring saturated pores adjacent to free pores. The clog growth rate is linked to the effective concentration of the suspension flowing through the pore: $v_N^* \propto \langle\phi_k\rangle_N Q_f$[10]. Finally, the ratio of clog growth rate with N clogged pores to clog growth rate with no clogged pore can be written as:

$$\frac{v_N^*}{v_0^*} = 1 + \langle k\rangle_N\frac{Q_s}{2Q_f}, \tag{3}$$

with $\langle k\rangle_N$ computed using a tree diagram approach (see Supplementary materials 3).

The flow rate Q_f is determined as already explained. The flow rate Q_s through a porous clog depends on its hydraulic resistance R_h^{clog}, which can be estimated using the Blake-Kozeny equation[31]:

$$R_h^{clog} = \frac{150\ell\eta(1-\varepsilon)^2}{whd_p\varepsilon^3}, \tag{4}$$

where ε represents the clog porosity, η the fluid dynamic viscosity, and ℓ a typical length of the clog. To estimate ℓ, we consider that, because they form in a corner, the clogs are roughly quarter-spheres, and assume that the radius of the clog corresponds to ℓ. Using the projected area at saturation, we obtain $\ell \sim 7\ \mu$m. The porosity can be estimated from a previous study[24], which shows that for pH = 6 (close to that in the present study), and for a small filtration cake of colloids, the porosity can reach $\varepsilon = 0.83$. This value is in good agreement with macroscopic measurements made by Brenner[20]. With these parameters, the hydraulic resistance estimate is $R_h^{clog} \approx 2 \times 10^{17}$ kg.m^{-4}.s^{-1}. The hydraulic resistance of the rectangular pore is very similar: $R_h^{slit} = 2.3 \times 10^{17}$ kg.m^{-4}.s^{-1}[30]. The resulting flow rate Q_s through a saturated pore will be about one-half of that in a free pore: $Q_s/Q_f \approx 0.5$. This value is of the same order of magnitude as the velocity decrease before clogging observed in the case of polymersome clogs (Fig. 4).

Discussion and Conclusion

The result of the model given by Eq. 3 is plotted as a solid line in Fig. 3. This model contains no free parameter: $\langle k\rangle_N$ is computed numerically and the ratio Q_s/Q_f is estimated on solid grounds. The model is in relatively good agreement with the experimental data. A key point, observed experimentally and well predicted by the model, is that the cross-talk between pores becomes more and more important as N increases. The clogging of a free pore will be influenced by a distant, saturated pore, if there are only saturated pores between them. To support this point, Fig. 3 also shows the results of the model obtained considering only the first one, two, three and four adjacent neighbour(s) in each direction to compute $\langle k\rangle_N$. We observe the convergence of these curves towards the full model (solid line), where the influence of all successive saturated neighbours is taken into account, which highlights the "long-range" cross-talk between pores captured in the model. Note that because of large error bars at large N, this cannot be decreed as the only valid model.

To summarize and conclude, we have directly imaged a fixed-pressure-drop filtration process of Brownian particles through nanoslits, leading to the formation of clogs at the nanoslits entrance. The observation of cross-talk between pores, with an increase of clog growth rate with the number of saturated pores, is the central

point of this paper. To the authors' knowledge, this is the first time such an experimental observation is reported. Such a result will certainly impact the current understanding of membrane fouling dynamics. The direct access to phenomena at this scale provided by the microfabrication, imaging, and flow control, together with a systematic data analysis method thus enables us to demonstrate an original basic phenomenon, i.e. the cross-talk between pores in colloidal filtration.

To better explain the cross-talk physics, several experimental parameters should be varied. First, tuning the "strength" of Brownian diffusion will assess the role of this mechanism on the redistribution of the particles along the membrane. Using less viscous fluids or smaller colloidal particles would allow access to the smaller Péclet numbers needed to explore this issue. Tuning the chip geometry is a second one. For instance, an increase of the pore period δ should have a direct influence on the cross-talk: at a given Brownian diffusion magnitude, the diffusion time scale between pores may become too large to allow for cross-talk. Another important quantity for the model is the flow rate Q_s through a saturated pore. It depends on the clog saturation size and internal structure, which both result from a balance between drag forces and repulsive interactions between the accumulated Brownian particles. Tuning the internal clog structure is then an interesting perspective. This may be achieved by changing the suspension salinity. For instance, at low ionic force, the repulsive interactions between particles, and thus the "effective volume" occupied by each of them, will be higher. It could lead to a less dense and more permeable clog which should increase the cross-talk effect. Work along these directions is currently in progress, even if made tricky by the challenges that are inherent to such experiments, as discussed in the experimental method section. Another interesting study could be to increase the particle volume fraction to observe possible collective diffusion influence on the cross-talk phenomenon. Finally, the model presented in this paper could be extended to different geometries, particularly 2-D membranes. This configuration could reduce the cross-talk effect because of the more important number of neighbours, limited to two in our 1-D experiment (so the factor 1/2 in the right-hand side term of Eq. 4). It will also impact the computation of $\langle k \rangle_N$. Nevertheless, it would be interesting to make similar measurements on 2-D membranes, such as microsieves, with different pore patterns and compare with the predictions of the phenomenological model.

References

1. Tavakkoli, M. *et al*. Indirect Method: A Novel Technique for Experimental Determination of Asphaltene Precipitation. *Energy & Fuels* **29**, 2890–2900, https://doi.org/10.1021/ef502188u (2015).
2. Fuller, S. B., Wilhelm, E. J. & Jacobson, J. M. Ink-jet printed nanoparticle microelectromechanical systems. *Journal of Microelectromechanical systems* **11**, 54–60, http://ieeexplore.ieee.org/abstract/document/982863/ (2002).
3. Rothberg, M. B. Coronary Artery Disease as Clogged Pipes: A Misconceptual Model. *Circulation: Cardiovascular Quality and Outcomes* **6**, 129–132, https://doi.org/10.1161/CIRCOUTCOMES.112.967778 (2013).
4. Pang, L. *et al*. Deformability and size-based cancer cell separation using an integrated microfluidic device. *The Analyst* **140**, 7335–7346, https://doi.org/10.1039/C5AN00799B (2015).
5. Zhang, W., Tang, X., Weisbrod, N. & Guan, Z. A review of colloid transport in fractured rocks. *Journal of Mountain Science* **9**, 770–787, https://doi.org/10.1007/s11629-012-2443-1 (2012).
6. Hilgers, C. & Urai, J. L. Experimental study of syntaxial vein growth during lateral fluid flow in transmitted light: first results. *Journal of Structural Geology* **24**, 1029–1043 (2002).
7. Dressaire, E. & Sauret, A. Clogging of microfluidic systems. *Soft Matter* **13**, 37–48, https://doi.org/10.1039/C6SM01879C (2017).
8. Sauret, A. *et al*. Clogging by sieving in microchannels: Application to the detection of contaminants in colloidal suspensions. *Applied Physics Letters* **105**, 074101, https://doi.org/10.1063/1.4893459 (2014).
9. Zuriguel, I. *et al*. Clogging transition of many-particle systems flowing through bottlenecks. *Scientific Reports* **4**, 7324, https://doi.org/10.1038/srep07324 (2014).
10. Wyss, H. M., Blair, D. L., Morris, J. F., Stone, H. A. & Weitz, D. A. Mechanism for clogging of microchannels. *Physical Review E* **74** https://doi.org/10.1103/PhysRevE.74.061402 (2006).
11. Dersoir, B., de Saint Vincent, M. R., Abkarian, M. & Tabuteau, H. Clogging of a single pore by colloidal particles. *Microfluidics and Nanofluidics* **19**, 953–961, https://doi.org/10.1007/s10404-015-1624-y (2015).
12. Bacchin, P., Marty, A., Duru, P., Meireles, M. & Aimar, P. Colloidal surface interactions and membrane fouling: Investigations at pore scale. *Advances in Colloid and Interface Science* **164**, 2–11, http://linkinghub.elsevier.com/retrieve/pii/S0001868610001922 https://doi.org/10.1016/j.cis.2010.10.005 (2011).
13. Duru, P. & Hallez, Y. A Three-Step Scenario Involved in Particle Capture on a Pore Edge. *Langmuir* **31**, 8310–8317, https://doi.org/10.1021/acs.langmuir.5b01298 (2015).
14. Robert de Saint Vincent, M., Abkarian, M. & Tabuteau, H. Dynamics of colloid accumulation under flow over porous obstacles. *Soft Matter* **12**, 1041–1050, https://doi.org/10.1039/C5SM01952D (2016).
15. Dersoir, B., Schofield, A. B. & Tabuteau, H. Clogging transition induced by self filtration in a slit pore. *Soft Matter* **13**, 2054–2066, https://doi.org/10.1039/C6SM02605B (2017).
16. Cejas, C. M., Monti, F., Truchet, M., Burnouf, J.-P. & Tabeling, P. Particle Deposition Kinetics of Colloidal Suspensions in Microchannels at High Ionic Strength. *Langmuir* **33**, 6471–6480, https://doi.org/10.1021/acs.langmuir.7b01394 (2017).
17. Kim, Y., Ahn, K. H. & Lee, S. J. Clogging mechanism of poly(styrene) particles in the flow through a single micro-pore. *Journal of Membrane Science* **534**, 25–32, http://linkinghub.elsevier.com/retrieve/pii/S0376738817303757 https://doi.org/10.1016/j.memsci.2017.04.010 (2017).
18. Laar, T. v. d., Klooster, S. t., Schroën, K. & Sprakel, J. Transition-state theory predicts clogging at the microscale. *Scientific Reports* **6** https://doi.org/10.1038/srep28450 (2016).
19. Sendekie, Z. B. & Bacchin, P. Colloidal Jamming Dynamics in Microchannel Bottlenecks. *Langmuir* **32**, 1478–1488, https://doi.org/10.1021/acs.langmuir.5b04218 (2016).
20. Brenner, H. Three-dimensional filtration on a circular leaf. *AIChE Journal* **7**, 666–671 (1961).
21. Ghidaglia, C., de Arcangelis, L., Hinch, J. & Guazzelli, É. Transition in particle capture in deep bed filtration. *Physical Review E* **53**, R3028, https://doi.org/10.1103/PhysRevE.53.R3028. (1996).
22. Narayan, R., Coury, J. R., Masliyah, J. H. & Gray, M. R. Particle capture and plugging in packed-bed reactors. *Industrial & engineering chemistry research* **36**, 4620–4627, https://doi.org/10.1021/ie970101e. (1997).
23. Hong, S., Faibish, R. S. & Elimielech, M. Kinetics of Permeate Flux Decline in Crossflow Membrane Filtration of Colloidal Suspensions. *Journal of Colloid ans Interface Science* **196**, 267–277 (1997).
24. Hieke, M., Ruland, J., Anlauf, H. & Nirschl, H. Analysis of the Porosity of Filter Cakes Obtained by Filtration of Colloidal Suspensions. *Chemical Engineering & Technology* **32**, 1095–1101, https://doi.org/10.1002/ceat.200800609 (2009).

25. Song, L. & Elimelech, M. Theory of concentration polarization in crossflow filtration. *Journal of the Chemical Society, Faraday Transactions* **91**, 3389–3398 (1995).
26. Bacchin, P., Meireles, M. & Aimar, P. Modelling of filtration: from the polarised layer to deposit formation and compaction. *Desalination* **145**, 139–146, https://hal.archives-ouvertes.fr/hal-00201115 https://doi.org/10.1016/S0011-9164(02)00399-5 (2002).
27. Shin, S., Ault, J. T., Warren, P. B. & Stone, H. A. Accumulation of Colloidal Particles in Flow Junctions Induced by Fluid Flow and Diffusiophoresis. *Physical Review X* **7**, https://doi.org/10.1103/PhysRevX.7.041038 (2017).
28. Liot, O. *et al.* Transport of nano-objects in narrow channels: influence of Brownian diffusion, confinement and particle nature. *Journal of Physics: Condensed Matter* **30**, 234001, https://doi.org/10.1088/1361-648X/aac0af (2018).
29. Cussler, E. L. *Diffusion: Mass Transfer in Fluid Systems* Google-Books-ID: dq6LdJyN8ScC.(Cambridge University Press, 2009).
30. Bruus, H. *Theoretical microfluidics* (Oxford university press Oxford, 2007). http://web-files.ait.dtu.dk/bruus/TMF/publications/books/Bruus_TMFbook_Sample_Chapter.pdf.
31. Bird, R. B. Transport phenomena. *Applied Mechanics Reviews* **55**, R1–R4, https://doi.org/10.1115/1.1424298 (2002).

Acknowledgements

We acknowledge the Fédération FERMaT and University of Toulouse (Project NEMESIS) for funding these researches. O. Liot warmly acknowledges M. Socol for his chip microfabrication and experimental help. This work was partly supported by LAAS-CNRS micro and nanotechnologies platform member of the French RENATECH network.

Author Contributions

O.L. and A.S. performed experiments and analysis. O.L. developed the model with P.D. P.J. and O.L. fabricated the microfluidic chips and assembled the experimental device. J.F.M. led the scientific project development within the context of the NEMESIS Chaire d'Attractivité at University of Toulouse. O.L. led the manuscript writing with inputs from P.D. and in which P.B., J.F.M. and P.J. took part.

Additional Information

Supplementary information accompanies this paper at https://doi.org/10.1038/s41598-018-30389-7.

Competing Interests: The authors declare no competing interests.

Publisher's note: Springer Nature remains neutral with regard to jurisdictional claims in published maps and institutional affiliations.